JGR Space Physics

RESEARCH ARTICLE
10.1029/2024JA032850

Jupiter's Whistler-Mode Belts and Electron Slot Region

Y.-X. Hao[1,2], Y. Y. Shprits[1,3,4], J. D. Menietti[5], Z. Y. Liu[6], T. Averkamp[5], D. D. Wang[1], P. Kollmann[7], G. B. Hospodarsky[5], A. Drozdov[4], E. Roussos[2], N. Krupp[2], R. B. Horne[8], E. E. Woodfield[8], and S. J. Bolton[9]

[1]GFZ German Research Centre for Geosciences, Potsdam, Germany, [2]Max Planck Institute for Solar System Research, Goettingen, Germany, [3]Institute of Physics and Astrophysics, University of Potsdam, Potsdam, Germany, [4]University of California Los Angeles, Los Angeles, CA, USA, [5]Department of Physics and Astronomy, University of Iowa, Iowa, IA, USA, [6]IRAP, CNRS-Universite Toulouse III Paul Sabatier, Toulouse, France, [7]Johns Hopkins University Applied Physics Laboratory, Laurel, MD, USA, [8]British Antarctic Survey, Cambridge, UK, [9]Space Science and Engineering Division, Southwest Research Institute, San Antonio, TX, USA

Key Points:

- A double-belt structure in Jovian whistler-mode wave (>0.1 f_{ceq}) intensity is revealed
- Near-equatorial energetic electron distributions measured by JEDI show similar radial and azimuthal profile as whistler-mode waves
- The dawn-dusk asymmetry in the outer whistler-mode belt intensity corresponds to either the abundance of source electrons or auroral hiss

Supporting Information:

Supporting Information may be found in the online version of this article.

Correspondence to:

Y.-X. Hao,
hao@mps.mpg.de

Citation:

Hao, Y.-X., Shprits, Y. Y., Menietti, J. D., Liu, Z. Y., Averkamp, T., Wang, D. D., et al. (2024). Jupiter's whistler-mode belts and electron slot region. *Journal of Geophysical Research: Space Physics*, *129*, e2024JA032850. https://doi.org/10.1029/2024JA032850

Received 2 MAY 2024
Accepted 26 NOV 2024

Abstract

The spatial distribution of whistler-mode wave emissions in the Jovian magnetosphere measured during the first 45 perijove orbits of Juno is investigated. A double-belt structure in whistler-mode wave intensity is revealed. Between the two whistler-mode belts, there exists a region devoid of 100 s keV electrons near the magnetic equator at $9 < M < 16$. Insufficient source electron population in such an electron "slot" region is a possible explanation for the relatively lower wave activity compared to the whistler-mode belts. The wave intensity of the outer whistler-mode belt measured in the dusk-premidnight sector is significantly stronger than in the postmidnight-dawn sector. We suggest that the inherent dawn-dusk asymmetries in source electron distribution and/or auroral hiss emission rather than the modulation of solar cycle are more likely to result in the azimuthal variation of outer whistler-mode belt intensity during the first 45 Juno perijove orbits.

Plain Language Summary

Whistler-mode waves act as a potential driver of energetic electron dynamics in the Jovian magnetosphere. By resonating with the gyro-bounce motion of electrons along the field line, whistler-mode waves lead to either the acceleration of electrons or their precipitation to the atmosphere. Quantifying the net effect of such waves toward the radiation belt of Jupiter requires a comprehensive knowledge of how wavers are distributed in the Jovian magnetosphere. With NASA's Juno mission, we reveal a novel double-belt distribution of the whistler-mode waves. Between the inner and outer whistler-mode belts there is a region lacking near-equatorial energetic (100 s keV) electrons. The outer whistler-mode belt seems to be a mixture of chorus waves generated near the equator and auroral hiss waves propagating from the polar region. Either more abundant source electrons at the duskside magnetic equator for chorus emission or stronger auroral hiss from the duskside polar region can explain the dawn-dusk asymmetry of the outer whistler-mode belt.

1. Introduction

As the magnetosphere with the most intense radiation belt(s) (e.g., B. Mauk & Fox, 2010) in our solar system, the Jovian magnetosphere is an attractive natural laboratory for studying wave-particle interactions. Plasma waves with a frequency ranging from below the ion cyclotron frequency (e.g., Alfvén waves (Saur et al., 2018)) to above the electron cyclotron frequency (e.g., Z-mode waves (Menietti, Yoon, et al., 2023)) contribute considerably to the dynamics of Jovian energetic electrons. Whistler-mode chorus and hiss waves, which have been demonstrated as key components to the terrestrial electron belt dynamics (Allison et al., 2021; Horne et al., 2005; Li et al., 2015; Zhao et al., 2019), are also key drivers of acceleration and loss of energetic electrons trapped in Jupiter's magnetic field (Horne et al., 2008; Y. Shprits et al., 2012; Woodfield et al., 2014).

Whistler-mode waves can drive both electron acceleration and loss. The quantification of their spatial and spectral distributions is necessary for evaluating their impact at Jupiter. A subset of measurements based on Galileo and Juno mission data (Li et al., 2020; Menietti, Averkamp, Imai, et al., 2021; Menietti, Averkamp, Kurth, et al., 2021; Menietti et al., 2012) have been analyzed. With the Juno Extended Mission updated to the 45th perijove orbits (PJ45) (e.g., Menietti, Averkamp, et al., 2023), a larger section of the nightside Jovian magnetosphere within $25R_J$ (R_J denotes Jupiter radius) has been sampled, giving us the opportunity to build a more comprehensive global map of whistle-mode waves.

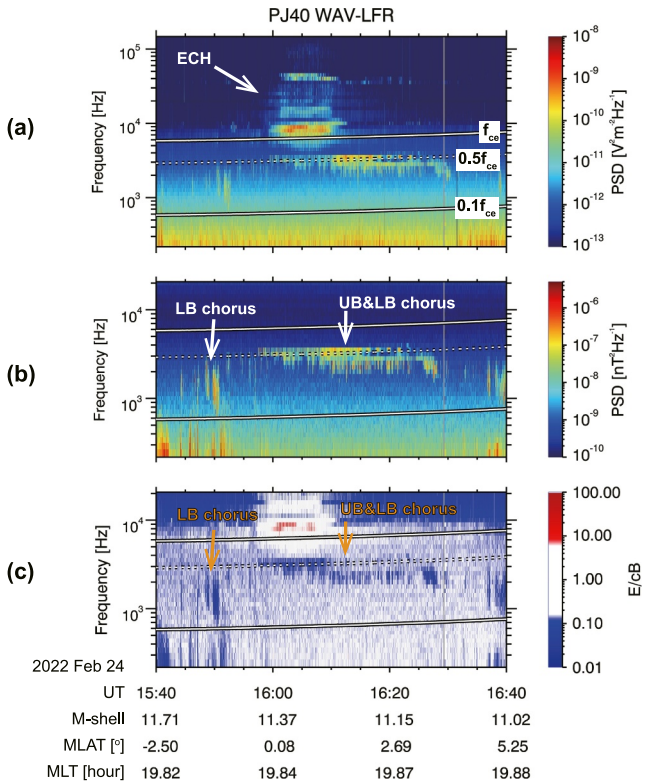

Figure 1. An example of whistler-mode chorus waves observed by Juno near the magnetic equator of Jupiter. (a) Wave electrical power spectral density (PSD), (b) Wave magnetic PSD, (c) E/cB during a magnetic equator passage of Juno's PJ40 orbit, showing ECH waves, lower-band (LB) and upper-band (UB) chorus. White curves in each panel indicate local f_{ce}, $0.5f_{ce}$ and $0.1f_{ce}$ values.

In this study, we focus on the spatial distribution of whistler-mode waves and their links to 30–800 keV electron spectra within $25R_J$, as measured by Juno during its first 45 perijove orbits. Unless otherwise stated, the wave frequency range is restricted to between $0.1f_{ceq}$ and $0.8f_{ceq}$ (f_{ceq} denotes the frequency of the equatorial electron cyclotron), whereas mapped energetic electron fluxes are selected within 4° of magnetic latitude. With the given frequency range, we highlight the spatial distribution of whistler-mode chorus waves, even if the contribution of auroral hiss waves cannot be fully excluded. Corresponding energetic electron measurements near the magnetic equator, where whistler-mode chorus waves are believed to be excited, are also analyzed for context. Additionally, the spatial distribution of whistler-mode waves studied here serves as the basis for a companion paper (Hao et al., 2024), which explores the acceleration of electrons driven by these waves.

2. Banded Chorus Waves Observed at the Magnetic Equator

Figure 1 shows an example of whistler-mode chorus emission measured by the Juno spacecraft near Jupiter's magnetic equator. The top/middle panel displays the electric/magnetic spectral density detected by the Juno Waves instrument (W. Kurth et al., 2017) while the bottom panel shows their ratio E/cB, where c is the speed of light. For electromagnetic waves propagating in vacuum, $E/cB = 1$ always holds. For waves propagating in magnetized plasma, E/cB can deviate from 1 due to the presence of various plasma effects. Certain wave modes (e.g., Langmuir waves) can exhibit $E/cB > 1$ due to their electrostatic nature. In terms of whistler-mode waves, the highly oblique wave (e.g., auroral hiss waves generated near the resonant cone) can also be quasi-electrostatic and show a large E/cB value (D. A. Gurnett, 1989). In the Juno measurement presented in Figure 1, the harmonic structure above the local electron cyclotron frequency f_{ce} (calculated with in-situ Juno magnetometer measurements (Connerney et al., 2017)) was observed between ~16:00–16:15, during a magnetic equator crossing. Large E/cB values indicate waves of an electrostatic nature. We note that such equatorial electrostatic waves with harmonic structure are tell-tale signatures of the electron cyclotron harmonics (ECH) emissions confined within the plasma sheet of Jupiter (cf., Menietti et al., 2012, Figure 4).

In addition to ECH emissions above f_{ce}, emissions between $0.1f_{ce}$ and $0.8f_{ce}$ are also recorded in Figure 1. The calculated $E/cB < 1$ indicates the clear electromagnetic nature of these waves. According to the Faraday law, $E/cB = 1/n\sin\beta$, where $n = c/v$ is the refractive index defined by the ratio of c to the wave phase velocity v (Stix, 1992) and β is the angle between the electric field of the wave and the wave propagation vector (Ni et al., 2011). In Jovian magnetosphere, Alfvén waves and magnetosonic waves have a phase velocity much smaller than c and therefore show $E/cB < 1$. As for quasi-parallel propagating whistler-mode waves in Jovian magnetosphere (i.e., chorus waves and broadband hiss waves), $E/cB < \sim 1$ are expected (Li et al., 2020). Note that the frequency range and E/cB value are typical for whistler-mode chorus waves detected by Juno Wave instrument (cf., Li et al., 2020, Figure 1) and cf., Menietti, Averkamp, Kurth, et al., 2021, Figure 1). At 15:45-15:55, the emission was confined between $0.1f_{ce}$ and $0.5f_{ce}$, is identified as typical lower band chorus waves. At 16:00–16:26, wave emissions were observed in both the $0.1f_{ce} - 0.5f_{ce}$ and $0.5f_{ce} - 1.0f_{ce}$ bands. Burst mode data of the Juno Waves instrument indicate that there existed a distinct power gap between the two frequency bands below and above $0.5f_{ce}$. Waves with such dual-band structure are reminiscent of whistler-mode chorus waves in the terrestrial magnetosphere (e.g., Teng et al., 2019; Tsurutani & Smith, 1974).

3. Global Morphology of Whistler-Mode Waves

Previous Juno-based studies (Li et al., 2020; Menietti, Averkamp, et al., 2023; Menietti, Averkamp, Imai, et al., 2021; Menietti, Averkamp, Kurth, et al., 2021) presented the spatial distribution of whistler-mode waves integrated power using f_{lh} or f_{ci} as the lower cutoff frequency (f_{lhr}: lower hybrid resonance, f_{ci} ion cyclotron frequency). We note that in these studies, wave intensities between the lower cutoff and $0.1f_{ce}$, which are likely to be (auroral) hiss waves, are much stronger than the wave intensities above $0.1f_{ce}$ (e.g., Li et al., 2020, Figure 4) (Menietti, Averkamp, Kurth, et al., 2021, Figure 5). Therefore, the global distributions of the integrated whistler-mode wave intensity in Li et al. (2020) and Menietti, Averkamp, Kurth, et al. (2021) mostly depict the wave morphology below $0.1f_{ce}$. As discussed in Section 2, Juno measurements demonstrate two points that we adopt in the upcoming sections: 1. Whistler-mode chorus waves in the Jovian magnetosphere show a distinct frequency band structure similar to the terrestrial chorus waves (Burtis & Helliwell, 1969); 2. The electron cyclotron frequency $\left(f_{ceq}\right)$ could be a suitable normalization factor for the spectrum of Jovian chorus waves (Menietti, Averkamp, Imai, et al., 2021; Menietti, Averkamp, Kurth, et al., 2021), as done for terrestrial chorus waves (e.g., *D*. Wang et al., 2019).

We focus on the spatial distribution of whistler-mode waves with the frequency range 0.1–$0.8f_{ceq}$, which is in the frequency range of "typical chorus waves" (e.g., Tsurutani & Smith, 1977; Meredith et al., 2012; *D*. Wang et al., 2019). We follow the same methodology as for the whistler-mode survey as in Menietti, Averkamp, Imai, et al. (2021) with data up to PJ45 (Menietti, Averkamp, et al., 2023). The same spatial grid size is adopted ($\Delta M = 1.0$, $\Delta MLT = 1h$, $\Delta\lambda = 2°$ for $|\lambda| < 16°$ and $\lambda = 5°$ for $|\lambda| > 16°$, where M, MLT and λ denote the M shell, magnetic local time, and magnetic latitude, respectively) for spatial binning. The M-shell and f_{ceq} are based on the JRM09 plus current sheet model (Connerney et al., 1981, 2018). Spatial grids and the accumulative sampling time of Juno per bin are shown in Figure S1 in Supporting Information S1. In this study, the outermost M-shell extends to 25, while the absolute value of magnetic latitude to 36°. Higher latitudes are excluded to minimize the influence of auroral hiss (e.g., Li et al., 2020, Figure 4). In terms of MLT, the whole night sector of Jupiter is covered.

The integrated wave intensity $\langle B_W^2 \rangle$ in each step of spacecraft sampling (hereafter referred to as "data point") is the average value of the wave intensity measured over the time interval $\Delta\tau = 1$ min. $\langle B_W^2 \rangle$ is calculated with

$$\langle B_W^2 \rangle = \langle \int_{uc}^{lc} PSD(f) df \rangle, \tag{1}$$

between $0.1f_{ceq}$ and $0.8f_{ceq}$ and $PSD(f)$ is the magnetic power spectral density. The frequency-resolved wave intensity $\langle B_{Wi}^2 \rangle$ is calculated within 7 normalized frequency $\left(\beta = f/f_{ceq}\right)$ bins using:

$$\langle B_{Wi}^2 \rangle = \langle \int_{\beta_i - \frac{1}{2}\Delta\beta}^{\beta_i + \frac{1}{2}\Delta\beta} PSD\left(f_{ceq}\,\beta\right) f_{ceq}\, d\beta \rangle, \tag{2}$$

in which each bin centers from $\beta_0 = 0.15$ to $\beta_7 = 0.75$ with the bandwidth $\Delta\beta = 0.1$. Figure 2 presents the spatial distribution of the average integrated magnetic intensity for whisler-mode waves in the chorus frequency range. Surprisingly, the spatial distribution of whistler-mode wave intensity in typical chorus frequency range exhibits a double-belt structure. In addition to the intense whistler-mode emission at $5 < M < 9$, another "whistler-mode belt" emerges at $18 < M < 25$, peaking at $M \approx 21$. The outer whistler-mode belt is of the strongest intensity around dusk, indicating a possible dawn-dusk asymmetry of the wave emission. Panels (b) and (c) show the intensity of whistler-mode emission in the meridian plane, averaged over midnight to dawn and dusk to midnight, respectively. Due to the orbital design of Juno, the sampling at $|\lambda| < 16°$, $M < 9$ was not sufficient to reveal the inner whistler-mode belt at dawn-to-midnight sector low-latitude region. For $16° < |\lambda| < 31°$ region, the drop in wave intensity is still visible at $9 < M < 16$ for the dawn-to-midnight sector. The outer whistler-mode belt is distinct in both sectors and extends at least up to $|\lambda| = 21°$. The outer belt whistler-mode wave intensity at the dusk-midnight sector is stronger in each corresponding $(M, |\lambda|)$ bin, suggesting that the observed dawn-dusk asymmetry is not due to an orbital bias.

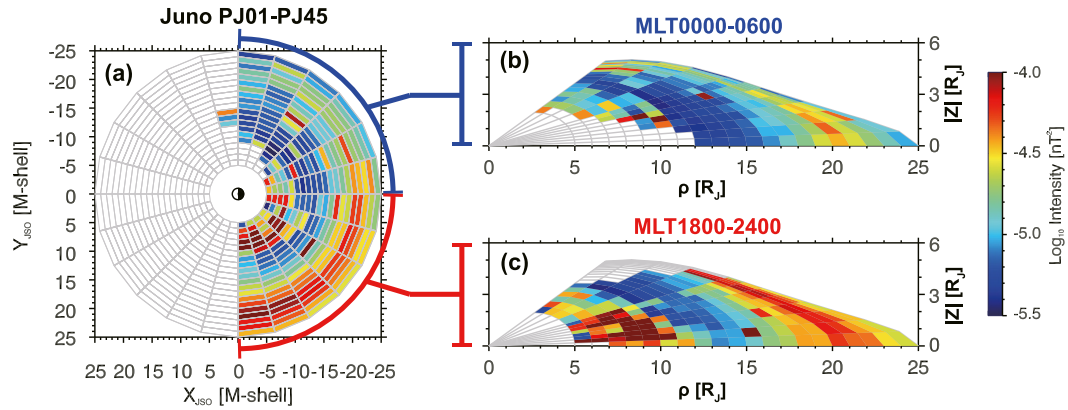

Figure 2. Whistler-mode wave intensity distribution. (a) M-shell versus MLT intensity spectrogram (b), (c) Wave intensity spectrogram in meridian plane for two MLT ranges. (c) Same format as panel (b) but for MLT from 1800 to 2400 (dusk-premidnight sector). Color coded are mean values of integrated wave intensity $\langle B_W^2 \rangle$ integrated between $0.1f_{ceq} < f < 0.8f_{ceq}$.

3.1. Double-Belt Structure of Whistler-Mode Wave Intensity

In Figure 3 we present the median, upper, and lower quartile of whistler-mode wave intensity as a function of M-shell. Since intense whistler-mode wave emissions have been reported during Ganymede and Europa flybys (D. Gurnett et al., 1996; Y. Y. Shprits et al., 2018; W. S. Kurth et al., 2022), possible Galilean-moon flybys have been excluded from our analysis.

As shown in Figure 3a, the median wave intensity of whistler-mode wave exhibits a distinct double-peaked distribution along the M-shell. The median value of integrated wave intensity at the belt peaks is comparable $\left(2 \times 10^{-5} nT^2 \sim 3 \times 10^{-5} nT^2\right)$. Note that outer peak is mainly visible in $f < 0.2f_{ceq}$ range, which contributes the most to the outer whistler-mode belt. For waves in $0.3f_{ceq} - 0.8f_{ceq}$ range, the intensity increases with M-shell monotonically between $11 < M < 25$. The "slot region" in between the two belts lies roughly between $M = 9$

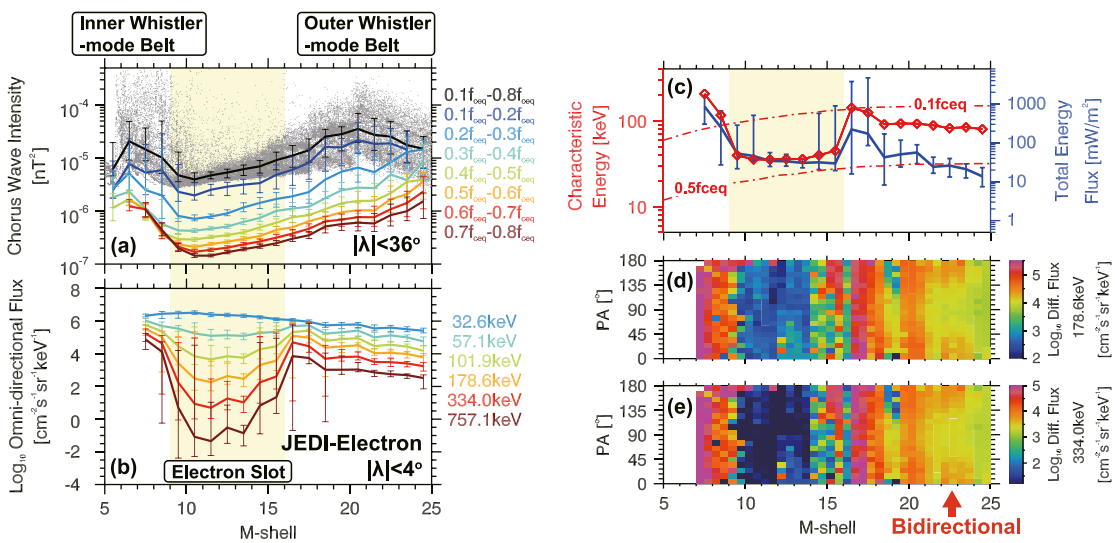

Figure 3. Statistical radial profile of whistler-mode waves and energetic electrons measured by Juno during orbits PJ01 through PJ45. (a) Whistler-mode wave intensity against M-shell. The gray points are 1 min averaged wave intensities. Solid curves present median values of wave intensity in each frequency bin (colored) and total integrated wave intensity (black). (b) Median omni-directional electron differential fluxes against M-shell measured near the magnetic equator. (c) Characteristic energy and total energy flux derived from JEDI measurements. Dashed-and-dotted curves show the minimum energy for cyclotron resonance between electrons and whistler-mode waves with the frequencies $0.1f_{ceq}$ and $0.5f_{ceq}$. The energetic electron slot is marked with light yellow. (d)–(e) Median pitch angle distribution of ~179 keV and ~334 keV electrons.

and 16 with an intensity minimum of one order of magnitude lower than at the peaks, located at $M \approx 11$. We further note that within the entire M-shell range, the highest contribution ot the integrated intensity comes for the $0.1f_{ceq} - 0.2f_{ceq}$ range. This statistical wave frequency spectrum is consistent with previous studies (cf., Figure 5b of Menietti, Averkamp, Kurth, et al. (2021)).

To explore the possible mechanisms behind the dual whistler-mode belt structure, we investigate the distribution of energetic electrons measured by Jupiter Energetic-particle Detector Instrument (Juno/JEDI) (B. Mauk, Haggerty, Jaskulek, et al., 2017), using publicly available data up to PJ44. As various studies (e.g., Burton & Holzer, 1974; Lauben et al., 2002; Tsurutani & Smith, 1977) have shown, whistler-mode chorus waves at Earth are excited near the magnetic equator, therefore, we focus on electrons populations measured within 4° of magnetic latitude. JEDI measurements during time intervals with "high resolution" spectra have been interpolated into the "low resolution" energy bins, assuming local power-law spectra between adjacent energy channels. Figure 3b presents the median-averaged distribution of omni-directional differential fluxes for 30–800 keV electrons within $M = 25$.

We note that there exists a slot-like region of energetic electrons between 9<M<16, where a flux depletion of 100 s keV electrons by over two orders of magnitude is identified. Such energy-dependent depletion was also seen partially in previous studies (e.g., J.-z. Wang et al., 2021, Figure 4). In Figure S2 in Supporting Information S1, we present both the median and mean values of the electron fluxes as a function of the M-shell measured during the first 29 (interval studied by Ma et al. (2021)) and 44 orbits (this study) of Juno. We note that due to the ascending perijove latitude of Juno, orbits PJ01-PJ29 did not cover the near-equator region at $M < 9$ and conclude that the slot's appearance is not an averaging method or data sampling artifact. Most notable is that the energetic electron slot coincides spatially with the region of low wave intensity between the inner and outer whistler-mode belts.

The colocation of the Jovian whistler-mode and energetic electrons slot regions is probably not a coincidence. Previous studies (Menietti, Averkamp, Imai, et al., 2021; Menietti, Averkamp, Kurth, et al., 2021) suggest that whistler-mode dynamics in the Jovian inner and middle magnetosphere is controlled by the intensity of 100 s keV electrons. The characteristic energy E_C, total energy flux ϵ_T (Clark et al., 2018; B. Mauk, Haggerty, Paranicas, et al., 2017) and pitch angle distribution (PAD) of energetic electrons are statistically derived to further depict the electron distribution profile. Minimum resonance energy (MRE) is calculated to estimate the energy range of source electrons for whistler-mode wave excitation.

The characteristic energy reflects the spectral hardness, while the total energy flux represents the energy budget of electrons, both of which are critical to the excitation of plasma waves. A source electron population with either a spectrum that is too soft or a total energy flux that is too low is not favorable for exciting whistler-mode waves. To examine the role of The characteristic energy of the electrons (B. Mauk et al., 2004) in a given energy range could be derived as

$$E_C = \frac{\int_{E_{\min}}^{E_{\max}} j \cdot E \, dE}{\int_{E_{\min}}^{E_{\max}} j \, dE}, \tag{3}$$

where j is the omni-directional differential flux and E is the kinetic energy of electrons measured by JEDI. Here we take $E_{\max} = 32.6keV$ and $E_{\min} = 757.1keV$ for a rough estimation. As shown in Figure 3c, the characteristic energy of the electron energy spectra drops steeply to $\sim 40keV$ at $M \approx 9$ and recovers to $\sim 100keV$ at $M \approx 16$, indicating much softer electron spectra inside the whistler-mode slot region than in the whistler-mode belts.

The total energy flux ϵ_T of the energetic electrons with the differential flux j(E) is calculated with

$$\epsilon_T = 4\pi \int_{E_{\min}}^{E_{\max}} j \cdot E \, dE. \tag{4}$$

The factor 4π is used for the omnidirectional electron population measured near the magnetic equator. The dark blue curve and error bars in Figure 3c show the median value, lower and upper quartile of ϵ_T as a function of M-shell. Sharp decreases in ϵ_T are distinct at $M \approx 9$ and $M \approx 16$, the boundaries of the electron slot region.

The energy range of source electrons to locally excite plasma waves can be estimated with the resonance condition. The cyclotron resonance condition between electrons and whistler-mode waves can be expressed as

$$\omega - k_{\parallel} v_{\parallel} = n|\Omega_e|/\gamma, \tag{5}$$

where $k_{\parallel}$ and $v_{\parallel}$ are the field-aligned components of the wave propagation vector and particle velocity, ω and $\Omega_e = 2\pi f_{ce}$ are the angular frequency of the wave and electrons, γ is the relativistic factor and $n = 0, \pm 1, \pm 2, \ldots$ is an integer referred to as the order of the cyclotron resonance.

Equation 5 is used to calculate the minimum resonant energy for the first-order cyclotron resonance ($n = 1$) between electrons and whistler-mode waves, which contribute to the growth and damping rates of whistler-mode chorus waves along with the Landau resonance ($n = 0$) (Kennel & Petschek, 1966; Li et al., 2010). A plasma density model derived from Voyager plasma measurements (Dougherty et al., 2017) is used, which shows good consistency with the latest Juno JADE measurements (J.-Z. Wang et al., 2024). The red curves in Figure 3c show the MRE for electrons in the $n = 1$ cyclotron resonance with the $f = 0.1 f_{ce}$ and $f = 0.5 f_{ce}$ field-aligned whistler-mode waves, respectively. Our calculation shows that for the $n = 1$ MRE for electrons and whistler-mode waves in the equatorial lower band chorus frequency range at the magnetic equator (the chorus source region) occurs in the 10–100 s of keV range at $5 \sim 25 R_J$. Such a minimum resonance energy is close to the estimated characteristic electron energy, indicating that the JEDI electron profile studied above is likely to be the source population of chorus waves. Note that the MRE calculated in Figure 3c provides only an estimate of the lower energy limit for an electron to enter the cyclotron resonance with a whistler-mode wave of a given frequency ($\alpha = 0°$, $n = 1$). Resonance at higher orders ($|n| > 1$) or for electrons with higher pitch angles corresponds to higher energies. Consequently, a broader range of electron energies above the MRE is capable of locally exciting whistler-mode waves. This may result in the higher frequency $\left(f > 0.5 f_{ceq}\right)$ wave profiles being more aligned with the characteristics of 100s keV electrons.

Panels (d) and (e) of Figure 3 present the statistical pitch angle distribution of electrons with an energy of ~178.6 keV and ~334.0 keV, respectively. Color-coded maps show the median value of the pitch-angle-resolved differential electron fluxes in each (M, α) grid ($\Delta M = 0.5$, $\Delta\alpha = 10°$), where α denotes the local pitch angle. For statistical electron PADs derived separately for the dawn-premidnight and postmidnight-dusk sectors, please refer to Figure S3 in Supporting Information S1, where additional energy channels are presented as well. We note that above $M = 21$, where the outer whistler-mode belt peaks, the bidirectional PAD distributions dominate, in agreement with Galileo observations (Tomás et al., 2004; B. H. Mauk & Saur, 2007) that a correlation between the PAD transition and the mapping of Jovian diffuse auroral emissions was indicated. Leakage of auroral hiss waves from the diffuse auroral zone may also contribute to the whistler-mode wave intensity in our statistics (detailed in Section 3.2). Saur et al. (2018) developed a theory of wave-particle interactions between kinetic Alfvén waves (KAWs) and electrons in the Jovian magnetosphere, suggesting that KAWs are capable of generating broadband bidirectional auroral electron beams. Further investigation of the relationship among whistler-mode waves, bidirectional electron beams, and KAWs is needed to reveal the mechanism of the outer-belt whistler-mode excitation and the Jovian diffuse-aurora emission.

3.2. Local-Time and Latitudinal Distribution of the Outer Whistler-Mode Belt

As shown in Figure 2, the Juno extended mission reveals a stronger outer whistler-mode belt measured in the dusk-premidnight sector than in the postmidnight-dawn sector. As it took more than 6 years for Juno to scan from MLT0600 to MLT1800, such a variation of wave intensity could either result from a temporal variation or a spatial asymmetry. In this section, both scenarios will be examined.

Figure S4a in Supporting Information S1 presents the solar wind speed and solar-disk Lyman-alpha intensity during the time interval of the Juno orbit PJ01-PJ45. For the first 45 orbits around Jupiter, Juno experienced both the descending phase of Solar Cycle 24 and the ascending phase of Solar Cycle 25. More high-speed solar wind events were recorded during the descending phase of Solar Cycle 24 than during the ascending phase of Solar Cycle 25. In contrast, the integrated wave power measured in the outer whistler-mode belt ($18 < M < 25$) increased almost monotonically from $6 \times 10^{-6} nT^2$ to $7 \times 10^{-6} nT^2$ (Figure S4b in Supporting Information S1). Long-term correlations between solar wind speed, solar-disk Lyman-alpha intensity, sunspot number, and outer-belt whistler-mode wave intensity are analyzed in Figure S4(c-e) in Supporting Information S1. The duration of

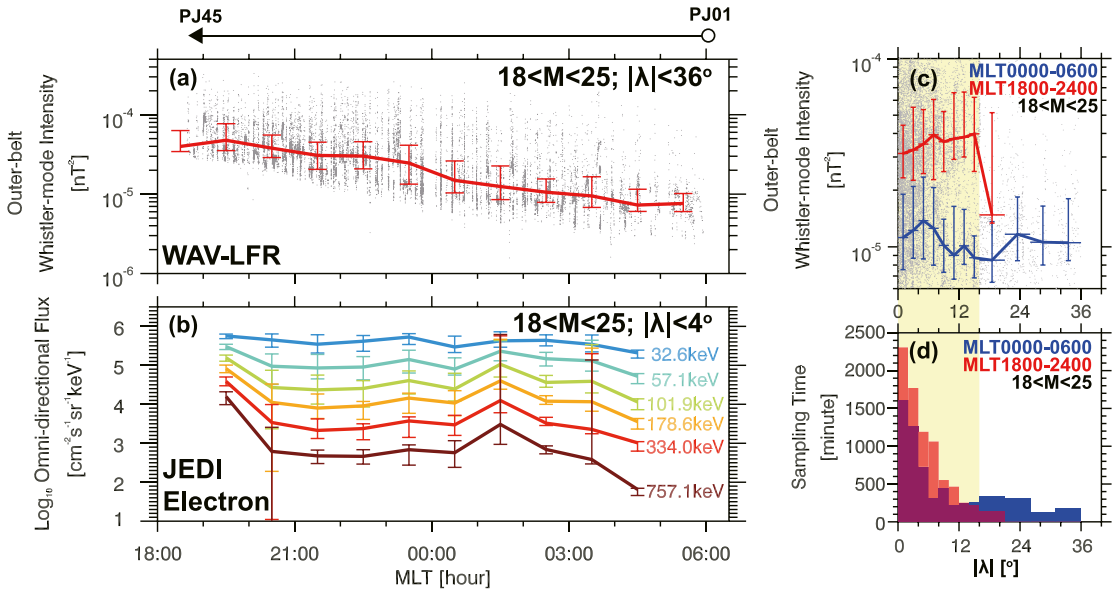

Figure 4. Local time asymmetry of the wave intensity and electron flux in the outer whistler-mode belt. (a) Whistler-mode wave intensity as a function of MLT. The solid curve shows the median wave intensity integrated from $0.1f_{ceq}$ to $0.8f_{ceq}$ within $18 < M < 25$ and $|\lambda| < 36°$. Gray points show the scatter plot of 1 min averaged, wave intensity integrated from $0.1f_{ceq}$ to $0.8f_{ceq}$. (b) Median, upper, and lower quartiles of omnidirectional electron fluxes as a function of the MLT measured near the magnetic equator. (c) Integrated wave intensity as a function of $|\lambda|$. Blue (red) curve denotes the median wave intensity sampled in the midnight-dawn (dusk-midnight) sector. Gray points are the same data as in panel (a) but plotted as against $|\lambda|$. (d) Sampling time as a function of $|\lambda|$ at $18 < M < 25$ in each MLT sector.

the time bin use for statistics is significantly longer than the time interval for solar wind to propagate to the Jovian magnetosphere. The analysis shows that similar conditions in solar wind velocity, Lyman-alpha intensity, or sunspot number can link to wave intensities differing by an order of magnitude. No clear positive or negative correlation between long-term solar activity and wave intensity is observed in our dataset. Therefore, the long-term intensity variation of the outer whistler-mode belt appears to be not significantly correlated with the solar cycles. The observed wave intensity variation is more likely to be an inherent dawn-dusk asymmetry in the Jovian magnetosphere.

Figure 4 presents the intensity of the outer whistler-mode belt and the energetic electron flux as a function of MLT. As the apogee of Juno precessed from dawn to dusk, both the integrated whistler-mode wave intensity and the energetic electron flux increased nearly monotonically. Dusk intensities are around seven times stronger than at dawn. A similar asymmetry trend is seen in energetic electrons (panel (b)). The energy spectrum measured at dusk is also harder than at dawn. Since near-equatorial of 10–100 s keV electrons are potential sources of outer-belt whistler-mode emissions (Section 3.1), we suggest that such dawn-dusk asymmetries in both waves and energetic electrons spectra are likely interconnected.

Another possible mechanism that may result in the local time asymmetry in outer-belt whistler-mode intensity is the dawn-dusk asymmetry in plasma density. Juno/JADE measurements in a similar time interval with our study reveal a potential local-time dependence on plasma density at $15 - 25R_J$ (cf., J.-Z. Wang et al., 2024, Figure 3a). Plasma density can affect the whistler-mode intensity by controlling its growth rate. Orbit-by-orbit study combining the plasma density, electron velocity distribution function and whistler-mode wave observations is needed to further understand the driving mechanism behind the spatial distribution of waves in Juno data.

It is worth noting that in the analysis above the contribution of auroral hiss waves cannot be fully eliminated (e.g., Li et al., 2020; Menietti, Averkamp, et al., 2023; Menietti, Averkamp, Kurth, et al., 2021). Auroral hiss has a source region in the auroral region and is observed by Juno at higher magnetic latitudes and M-shells, and can be observed for large distances from its origin (D. A. Gurnett et al., 1983; Sazhin et al., 1993). Menietti, Averkamp, et al. (2023) set a limit on the observations of Jovian chorus emission at $|\lambda| < 31°$ or $M < 20$. At a larger M-shell or higher magnetic latitude, auroral hiss waves could become the dominant source of whistler-mode emission. In Figure S5 in Supporting Information S1, we show an example of intense whistler-mode auroral hiss waves. This is distinguished by the spectrogram wave morphology in the top two panels of Figure S5 in Supporting

Information S1, showing a generally smooth appearance with no distinct narrow band signature as in the case of chorus waves. Chorus waves are known to have a source near the magnetic equator (cf. Hospodarsky et al. (2012)). The waves shown in Figure S5 in Supporting Information S1 propagate away from Jupiter and toward the magnetic equator, which is consistent with auroral hiss. This is shown by analyzing the phase of the waves relative to the E_y and B_z antennas of the Juno Waves plasma wave instrument, as described in Kolmašová et al. (2018).

Distinguishing auroral hiss waves from chorus waves with the method shown above requires burst-mode Juno Waves data, which are not always available for our study. Here we attempt to identify the contribution of chorus and auroral hiss from the latitudinal distribution of the wave intensity, shown in Figures 2b and 2c). For the inner whistler-mode belt ($M < 12$), strong whistler-mode emissions concentrate in the near-equatorial region. Therefore, the inner whistler-mode belt is more likely to be dominated by chorus waves. For the outer whistler-mode belt, in the midnight-dawn sector, there is also a peak of near-equatorial wave intensity ($|\lambda| < 8°$), indicating a possible contribution of chorus waves generated near the magnetic equator. In the dusk-midnight sector, the latitudinal dependence of the mean wave intensity is not clear. In Figure 4c, we further present the median value of wave intensity in the outer whistler-mode belt. In the midnight-dawn sector, the median value also shows a peak within $|\lambda| < 16°$, which is most likely to be near-equatorial chorus waves rather than auroral hiss waves. At $|\lambda| \approx 23.5°$, another peak of the median wave intensity appears, indicating the contribution of auroral hiss waves. In the dusk-pre-midnight sector, the median wave intensity increases with $|\lambda|$ in the region $0° \leq |\lambda| < 16°$ and drops dramatically at $|\lambda| \approx 18.5°$. We note that for the $|\lambda| > 16°$ region, the orbital coverage of Juno was limited in the dusk-midnight sector. Therefore, it is hard to derive a complete latitudinal dependence of the wave intensity in the dusk-midnight sector from the Juno measurements. Based on our analysis above, we suggest that the "outer whistler-mode belt" may consist of both equatorial chorus waves and auroral hiss waves from the Jovian polar region. The presence of whistler-mode waves that are not locally excited provides an alternative explanation to why the M-shell profile of $0.5 - 0.8 f_{ceq}$ waves does not resemble the M-shell profile of 30 keV electrons, which does not show an apparent slot region at $9 < M < 16$. The contribution of auroral hiss waves may also explain the increasing wave intensity in the frequency range $0.3 f_{ceq} < f < 0.8 f_{ceq}$ at $M > 11$ (see Figure 2a). As hiss emission is most likely to have a source in the auroral region where local $f_{ce} > f_{ceq}$, increasing contribution of auroral hiss emissions at larger M-shell may lead to the frequency-dependent trend in wave intensity at $11 < M < 25$. Orbit-by-orbit analysis of wave properties is needed to further reveal the physical nature of the intense wave emission at $18 < M < 25$.

4. Summary and Discussion

Using the Juno spacecraft during its primary and extended mission, we resolved several concurrent features in whistler-mode wave and energetic electron intensities.

1. There is a double-belt structure in the intensity of Jovian whistler-mode waves $\left(0.1 f_{ceq} < f < 0.8 f_{ceq}\right)$ between $M = 5$ and 25. An outer whistler-mode belt peaks at $M \approx 21$ and shows a wave intensity comparable to an inner whistler-mode belt at $M < 9$.
2. Between the aforementioned whistler-mode belts, a "slot" region of low energetic electron fluxes is revealed. At the region where $9 < M < 16$ and $|\lambda| < 4°$, the median fluxes of 100–700 keV electrons drop by over two orders of magnitude compared to the ambient environment. At $M \approx 21$, where the outer whistler-mode belt peaks, the pancake pitch angle distribution of 100 keV electrons switches to a bidirectional distribution.
3. The intensity of waves observed in the dusk-midnight sector of the outer whistler-mode belt is significantly higher than in the midnight-dawn sector. Fluxes of energetic electrons show a similar trend. Such distributions are most likely due to an inherent dawn-dusk asymmetry of the Jovian magnetosphere.
4. According to the latitudinal dependence of the wave intensity, the outer whistler-mode belt is a mixture of near-equatorial chorus waves and auroral hiss.

Since this study focused on the frequency range above $0.1 f_{ceq}$, it is no surprise that the spatial distribution patterns of wave intensity differ from previous studies starting from the local proton frequency $\left(f_{cp}\right)$ or the lower hybrid frequency $\left(f_{lh}\right)$, with which waves of lower frequency are counted (Li et al., 2020; Menietti, Averkamp, Imai, et al., 2021; Menietti, Averkamp, Kurth, et al., 2021).

Juno observations have shown that the global distribution patterns of whistler-mode waves and 100 s of keV electrons share mutual features in both the radial and azimuthal dimensions. Estimation of the minimum resonant energy for the $n = 1$ cyclotron resonance indicates that the aforementioned electron population is likely to be the source electrons that excite the whistler-mode waves. The mechanism that forms such an electron distribution map remains enigmatic. Some possible explanations are briefly discussed below.

A comprehensive analysis of phase space density (PSD) for the electron slot region requires calculating the second adiabatic invariant using a reliable magnetic field model, which is beyond the scope of this paper. However, the flux profile in this region suggests that the radial PSD profile is more complex than a simple monotonic increase or decrease toward the planet. The radial diffusion process alone cannot explain the presence of the electron slot. Losses (absorption, scattering) and/or local accelerations are needed. Wave-particle interactions at higher latitude (e.g., inside the auroral zone (Elliott et al., 2018; Saur et al., 2018)) or from frequencies different from those studied here (e.g., Z-mode waves (Menietti, Averkamp, Kurth, et al., 2021) or EMIC/hiss waves (Li et al., 2020)) may be responsible. Comprehensive Fokker-Planck simulations considering realistic wave species and distribution (Nénon et al., 2017) may help to understand the role of wave-particle interactions in the formation of the electron slot found in this study. We also highlight that the inner and outer edges of the electron slot are located at $M \approx 9$ and $M \approx 16$, which coincide with the orbits of Europa and Ganymede. For instance, at the outer edge of the electron slot ($M \approx 16$), electron fluxes from $\sim$60 keV to >700 keV decrease sharply toward the planet, indicating a steep positive PSD gradient for the corresponding first adiabatic invariants. This steep gradient may suggest the presence of a barrier or a sink that partially prevents energetic electrons beyond Ganymede's orbit from being transported inward by radial diffusion to smaller M-shells. It is important to note that moons produce intense whistler-mode wave emissions (Y. Y. Shprits et al., 2018; W. S. Kurth et al., 2022). These localized but very strong wave sources can drive local electron acceleration or loss (Y. Y. Shprits et al., 2018; Li et al., 2023) via wave-particle interaction, which could serve as a potential mechanism to generate the energetic electron slot region between these two moons.

Regarding the dawn-dusk electron flux asymmetry, several sources could serve as a potential explanation (Palmaerts et al., 2017, and references therein). The dawn-dusk asymmetry in the brightness of the Io torus (Murakami et al., 2016; Schneider & Trauger, 1995) is believed to be driven by the dawn-to-dusk electric field (Barbosa & Kivelson, 1983; Ip & Goertz, 1983). Such an electric field has also recently been utilized to explain the prompt acceleration of multi-MeV electrons at $M > 14R_J$ (Hao et al., 2020; Roussos et al., 2018; Yuan et al., 2021). The dawn-to-dusk electric field may also explain the higher flux and harder energy spectra observed by both Juno/JEDI (this study) and Galileo/EPD (Yuan et al., 2024) at dusk in comparison to the dawn flank. Another possible mechanism could be related to the corotation breakdown. Previous studies on ion flow anisotropies (Krupp et al., 2001; Waldrop et al., 2015) indicated that the corotation of the Jovian plasma starts to breakdown at $15 \sim 20R_J$ in the dusk sector, while remaining rigid or even supercorotational in the dawn sector. Corotation breakdown may supply the heating and increase in the anisotropy of energetic electrons and hence lead to stronger chorus wave emissions in the dusk magnetosphere. Theoretical studies (Kivelson & Southwood, 2005; Vogt et al., 2014) also discussed how centrifugal forces contribute to particle anisotropy and their local time asymmetry during outward expansion of flux tubes, which could also be related to dawn-dusk asymmetries in energetic electron distributions reported in this study.

Finally, the possibility that long-term temporal variations resulted in the observed inhomogeneity of the outer whistler-mode belt cannot be completely ruled out. It took 6.1 years for Juno to achieve the map shown in Figure 2a, approximately half of the orbital period of Jupiter (11.86 years). Although in Section 3.2 we have shown that the intensity of the outer whistler-mode belt is not clearly correlated with solar activity, the seasonal effect remains a potential explanation for the observed variations in the Juno data. Jupiter's relatively large orbital eccentricity (0.049) results in seasonal variations in solar irradiance, with a magnitude of approximately 20% (X. Wang et al., 2024). Recent studies have revealed potential long-term modulations in global radiant energy imbalances (Orton et al., 2023). However, it remains unclear how these radiant energy imbalances, which influence Jupiter's atmospheric system, may also modulate its magnetosphere. The strength of the coupling between the solar activity and the inner magnetosphere of Jupiter remains an open question as well. Furthermore, due to the lack of Juno equatorial coverage at MLT0000-0600 and $M < 12$, only the asymmetry of the outer whistler-mode belt is discussed in the present study. Combining Galileo data (e.g., Menietti et al., 2012; Y. Y. Shprits et al., 2018; Li et al., 2020) with Juno data may help to draw a more conclusive

picture of the whistler-mode wave distribution and temporal variation after undergoing the necessary cross-calibrations.

Data Availability Statement

Juno/JEDI data can be obtained at https://pds-ppi.igpp.ucla.edu/collection/JNO-J-JED-3-CDR-V1.0. Juno WAV data can be obtained at https://pds-ppi.igpp.ucla.edu/collection/JNO-E_J_SS-WAV-3-CDR-SRVFULL-V2.0:DATA. Solar wind speed data can be obtained at https://cdaweb.gsfc.nasa.gov/sp_phys/data/omni/hro_1min/. Solar Lyman-alpha intensity data can be obtained at https://cdaweb.gsfc.nasa.gov/sp_phys/data/omni/hro_1min/.

Acknowledgments
Y. Y. S, J. D. M and T. F. A are supported by the NASA Survey of Jovian Plasma Wave Intensity and Diffusive Modeling of Electron Acceleration and Scattering of Juno Participating Scientist Program (80NSSC19K1262). E. E. W is supported by the STFC (Science and Technology Facilities Council, UK) grant (ST/W00111X/1). Y. Y. S declares a potential con flict of in terest and significant financial interest in Space Sciences Innovations Inc. in Seattle, WA. The authors sincerely acknowledge Margaret G. Kivelson and Xianzhe Jia for the discussion section. Open Access funding enabled and organized by Projekt DEAL.

References

Allison, H. J., Shprits, Y. Y., Zhelavskaya, I. S., Wang, D., & Smirnov, A. G. (2021). Gyroresonant wave-particle interactions with chorus waves during extreme depletions of plasma density in the Van Allen radiation belts. *Science Advances*, *7*(5), eabc0380. https://doi.org/10.1126/sciadv.abc0380

Barbosa, D., & Kivelson, M. (1983). Dawn-dusk electric field asymmetry of the io plasma torus. *Geophysical Research Letters*, *10*(3), 210–213. https://doi.org/10.1029/gl010i003p00210

Burtis, W., & Helliwell, R. (1969). Banded chorus—A new type of VLF radiation observed in the magnetosphere by OGO 1 and OGO 3. *Journal of Geophysical Research*, *74*(11), 3002–3010. https://doi.org/10.1029/ja074i011p03002

Burton, R. K., & Holzer, R. E. (1974). The origin and propagation of chorus in the outer magnetosphere. *Journal of Geophysical Research*, *79*(7), 1014–1023. https://doi.org/10.1029/ja079i007p01014

Clark, G., Tao, C., Mauk, B., Nichols, J., Saur, J., Bunce, E., et al. (2018). Precipitating electron energy flux and characteristic energies in Jupiter's main auroral region as measured by Juno/JEDI. *Journal of Geophysical Research: Space Physics*, *123*(9), 7554–7567. https://doi.org/10.1029/2018ja025639

Connerney, J., Acuna, M., & Ness, N. (1981). Modeling the Jovian current sheet and inner magnetosphere. *Journal of Geophysical Research*, *86*(A10), 8370–8384. https://doi.org/10.1029/ja086ia10p08370

Connerney, J., Benn, M., Bjarno, J., Denver, T., Espley, J., Jorgensen, J., et al. (2017). The Juno magnetic field investigation. *Space Science Reviews*, *213*(1–4), 39–138. https://doi.org/10.1007/s11214-017-0334-z

Connerney, J., Kotsiaros, S., Oliversen, R., Espley, J., Joergensen, J. L., Joergensen, P., et al. (2018). A new model of jupiter's magnetic field from Juno's first nine orbits. *Geophysical Research Letters*, *45*(6), 2590–2596. https://doi.org/10.1002/2018gl077312

Dougherty, L. P., Bodisch, K. M., & Bagenal, F. (2017). Survey of voyager plasma science ions at jupiter: 2. Heavy ions. *Journal of Geophysical Research (Space Physics)*, *122*(8), 8257–8276. https://doi.org/10.1002/2017JA024053

Elliott, S., Gurnett, D., Kurth, W., Mauk, B., Ebert, R., Clark, G., et al. (2018). The acceleration of electrons to high energies over the Jovian polar cap via whistler mode wave-particle interactions. *Journal of Geophysical Research: Space Physics*, *123*(9), 7523–7533. https://doi.org/10.1029/2018ja025797

Gurnett, D., Kurth, W., Roux, A., Bolton, S., & Kennel, C. (1996). Evidence for a magnetosphere at Ganymede from plasma-wave observations by the Galileo spacecraft. *Nature*, *384*(6609), 535–537. https://doi.org/10.1038/384535a0

Gurnett, D. A. (1989). Auroral plasma waves. In *International conference on auroral physics*.

Gurnett, D. A., Shawhan, S. D., & Shaw, R. R. (1983). Auroral hiss, z mode radiation, and auroral kilometric radiation in the polar magnetosphere: DE 1 observations. *Journal of Geophysical Research*, *88*(A1), 329–340. https://doi.org/10.1029/ja088ia01p00329

Hao, Y.-X., Shprits, Y. Y., Menietti, J. D., Averkamp, T., Wang, D. D., Kollmann, P., et al. (2024). Acceleration of energetic electrons in Jovian middle magnetosphere by whistler-mode waves. *Journal of Geophysical Research: Space Physics*, *129*, e2024JA032735.https://doi.org/10.1029/2024JA032735

Hao, Y.-X., Sun, Y.-X., Roussos, E., Liu, Y., Kollmann, P., Yuan, C.-J., et al. (2020). The formation of Saturn's and jupiter's electron radiation belts by magnetospheric electric fields. *The Astrophysical Journal Letters*, *905*(1), L10. https://doi.org/10.3847/2041-8213/abca3f

Horne, R. B., Thorne, R. M., Glauert, S. A., Douglas Menietti, J., Shprits, Y. Y., & Gurnett, D. A. (2008). Gyro-resonant electron acceleration at Jupiter. *Nature Physics*, *4*(4), 301–304. https://doi.org/10.1038/nphys897

Horne, R. B., Thorne, R. M., Shprits, Y. Y., Meredith, N. P., Glauert, S. A., Smith, A. J., et al. (2005). Wave acceleration of electrons in the Van Allen radiation belts. *Nature*, *437*(7056), 227–230. https://doi.org/10.1038/nature03939

Hospodarsky, G., Sigsbee, K., Leisner, J., Menietti, J., Kurth, W., Gurnett, D., et al. (2012). Plasma wave observations at earth, jupiter, and saturn. *Dynamics of the Earth's Radiation Belts and Inner Magnetosphere*, *199*, 415–430. https://doi.org/10.1029/2012gm001342

Ip, W.-H., & Goertz, C. (1983). An interpretation of the dawn–dusk asymmetry of uv emission from the Io plasma torus. *Nature*, *302*(5905), 232–233. https://doi.org/10.1038/302232a0

Kennel, C. F., & Petschek, H. E. (1966). Limit on stably trapped particle fluxes. *Journal of Geophysical Research*, *71*(1), 1-+–28. https://doi.org/10.1029/jz071i001p00001

Kivelson, M., & Southwood, D. (2005). Dynamical consequences of two modes of centrifugal instability in Jupiter's outer magnetosphere. *Journal of Geophysical Research*, *110*(A12). https://doi.org/10.1029/2005ja011176

Kolmašová, I., Imai, M., Santolík, O., Kurth, W. S., Hospodarsky, G. B., Gurnett, D. A., et al. (2018). Discovery of rapid whistlers close to Jupiter implying lightning rates similar to those on earth. *Nature Astronomy*, *2*(7), 544–548. https://doi.org/10.1038/s41550-018-0442-z

Krupp, N., Lagg, A., Livi, S., Wilken, B., Woch, J., Roelof, E., & Williams, D. (2001). Global flows of energetic ions in Jupiter's equatorial plane: First-order approximation. *Journal of Geophysical Research*, *106*(A11), 26017–26032. https://doi.org/10.1029/2000ja900138

Kurth, W., Hospodarsky, G., Kirchner, D., Mokrzycki, B., Averkamp, T., Robison, W., et al. (2017). The Juno waves investigation. *Space Science Reviews*, *213*(1–4), 347–392. https://doi.org/10.1007/s11214-017-0396-y

Kurth, W. S., Sulaiman, A. H., Hospodarsky, G. B., Menietti, J. D., Mauk, B. H., Clark, G., et al. (2022). Juno plasma wave observations at Ganymede. *Geophysical Research Letters*, *49*(23), e2022GL098591. https://doi.org/10.1029/2022gl098591

Lauben, D. S., Inan, U. S., Bell, T. F., & Gurnett, D. (2002). Source characteristics of ELF/VLF chorus. *Journal of Geophysical Research*, *107*(A12), SMP–10. https://doi.org/10.1029/2000ja003019

Li, W., Ma, Q., Shen, X.-C., Zhang, X.-J., Mauk, B., Clark, G., et al. (2023). Driver of energetic electron precipitation in the vicinity of Ganymede. *Geophysical Research Letters*, *50*(6), e2022GL101555. https://doi.org/10.1029/2022gl101555

Li, W., Ma, Q., Thorne, R., Bortnik, J., Kletzing, C., Kurth, W., et al. (2015). Statistical properties of plasmaspheric hiss derived from Van Allen Probes data and their effects on radiation belt electron dynamics. *Journal of Geophysical Research: Space Physics*, *120*(5), 3393–3405. https://doi.org/10.1002/2015ja021048

Li, W., Shen, X.-C., Menietti, J., Ma, Q., Zhang, X.-J., Kurth, W., & Hospodarsky, G. (2020). Global distribution of whistler mode waves in jovian inner magnetosphere. *Geophysical Research Letters*, *47*(15), e2020GL088198. https://doi.org/10.1029/2020gl088198

Li, W., Thorne, R., Nishimura, Y., Bortnik, J., Angelopoulos, V., McFadden, J., et al. (2010). THEMIS analysis of observed equatorial electron distributions responsible for the chorus excitation. *Journal of Geophysical Research*, *115*(A6). https://doi.org/10.1029/2009ja014845

Ma, Q., Li, W., Zhang, X.-J., Shen, X.-C., Daly, A., Bortnik, J., et al. (2021). Energetic electron distributions near the magnetic equator in the Jovian plasma sheet and outer radiation belt using Juno observations. *Geophysical Research Letters*, *48*(24), e2021GL095833. https://doi.org/10.1029/2021gl095833

Mauk, B., & Fox, N. (2010). Electron radiation belts of the solar system. *Journal of Geophysical Research*, *115*(A12). https://doi.org/10.1029/2010ja015660

Mauk, B., Haggerty, D., Jaskulek, S., Schlemm, C., Brown, L., Cooper, S., et al. (2017a). The Jupiter energetic particle detector instrument (JEDI) investigation for the Juno mission. *Space Science Reviews*, *213*(1–4), 289–346. https://doi.org/10.1007/s11214-013-0025-3

Mauk, B., Haggerty, D., Paranicas, C., Clark, G., Kollmann, P., Rymer, A., et al. (2017b). Juno observations of energetic charged particles over Jupiter's polar regions: Analysis of monodirectional and bidirectional electron beams. *Geophysical Research Letters*, *44*(10), 4410–4418. https://doi.org/10.1002/2016gl072286

Mauk, B., Mitchell, D., McEntire, R., Paranicas, C., Roelof, E., Williams, D., et al. (2004). Energetic ion characteristics and neutral gas interactions in Jupiter's magnetosphere. *Journal of Geophysical Research*, *109*(A9). https://doi.org/10.1029/2003ja010270

Mauk, B. H., & Saur, J. (2007). Equatorial electron beams and auroral structuring at Jupiter. *Journal of Geophysical Research*, *112*(A10). https://doi.org/10.1029/2007ja012370

Menietti, J., Averkamp, T., Imai, M., Kurth, W., Clark, G., Allegrini, F., et al. (2021a). Low-latitude whistler-mode and higher-latitude Z-mode emission at Jupiter observed by Juno. *Journal of Geophysical Research: Space Physics*, *126*(2), e2020JA028742. https://doi.org/10.1029/2020ja028742

Menietti, J., Averkamp, T., Kurth, W., Faden, J., & Bolton, S. (2023a). Survey and analysis of whistler-and Z-mode emission in the Juno extended mission. *Journal of Geophysical Research: Space Physics*, *128*(12), e2023JA032037. https://doi.org/10.1029/2023ja032037

Menietti, J., Averkamp, T., Kurth, W., Imai, M., Faden, J., Hospodarsky, G., et al. (2021b). Analysis of whistler-mode and Z-mode emission in the Juno primary mission. *Journal of Geophysical Research: Space Physics*, *126*(11), e2021JA029885. https://doi.org/10.1029/2021ja029885

Menietti, J., Shprits, Y., Horne, R., Woodfield, E., Hospodarsky, G., & Gurnett, D. (2012). Chorus, ECH, and Z mode emissions observed at Jupiter and Saturn and possible electron acceleration. *Journal of Geophysical Research*, *117*(A12). https://doi.org/10.1029/2012ja018187

Menietti, J., Yoon, P., Averkamp, T., Kurth, W., Faden, J., Allegrini, F., et al. (2023b). Wave and particle analysis of Z-mode and O-mode emission in the Jovian inner magnetosphere. *Journal of Geophysical Research: Space Physics*, *128*(5), e2022JA031199. https://doi.org/10.1029/2022ja031199

Meredith, N. P., Horne, R. B., Sicard-Piet, A., Boscher, D., Yearby, K. H., Li, W., & Thorne, R. M. (2012). Global model of lower band and upper band chorus from multiple satellite observations. *Journal of Geophysical Research*, *117*(A10). https://doi.org/10.1029/2012ja017978

Murakami, G., Yoshioka, K., Yamazaki, A., Tsuchiya, F., Kimura, T., Tao, C., et al. (2016). Response of Jupiter's inner magnetosphere to the solar wind derived from extreme ultraviolet monitoring of the Io plasma torus. *Geophysical Research Letters*, *43*(24), 12–308. https://doi.org/10.1002/2016gl071675

Nénon, Q., Sicard, A., & Bourdarie, S. (2017). A new physical model of the electron radiation belts of Jupiter inside Europa's orbit. *Journal of Geophysical Research: Space Physics*, *122*(5), 5148–5167. https://doi.org/10.1002/2017ja023893

Ni, B., Thorne, R. M., Meredith, N. P., Shprits, Y. Y., & Horne, R. B. (2011). Diffuse auroral scattering by whistler mode chorus waves: Dependence on wave normal angle distribution. *Journal of Geophysical Research*, *116*(A10). https://doi.org/10.1029/2011ja016517

Orton, G. S., Antuñano, A., Fletcher, L. N., Sinclair, J. A., Momary, T. W., Fujiyoshi, T., et al. (2023). Unexpected long-term variability in Jupiter's tropospheric temperatures. *Nature Astronomy*, *7*(2), 190–197. https://doi.org/10.1038/s41550-022-01839-0

Palmaerts, B., Vogt, M. F., Krupp, N., Grodent, D., & Bonfond, B. (2017). Dawn-dusk asymmetries in Jupiter's magnetosphere. *Dawn-Dusk Asymmetries in Planetary Plasma Environments*, 307–322.

Roussos, E., Kollmann, P., Krupp, N., Paranicas, C., Dialynas, K., Sergis, N., et al. (2018). Drift-resonant, relativistic electron acceleration at the outer planets: Insights from the response of Saturn's radiation belts to magnetospheric storms. *Icarus*, *305*, 160–173. https://doi.org/10.1016/j.icarus.2018.01.016

Saur, J., Janser, S., Schreiner, A., Clark, G., Mauk, B. H., Kollmann, P., et al. (2018). Wave-particle interaction of Alfvén waves in Jupiter's magnetosphere: Auroral and magnetospheric particle acceleration. *Journal of Geophysical Research: Space Physics*, *123*(11), 9560–9573. https://doi.org/10.1029/2018ja025948

Sazhin, S., Bullough, K., & Hayakawa, M. (1993). Auroral hiss: A review. *Planetary and Space Science*, *41*(2), 153–166. https://doi.org/10.1016/0032-0633(93)90045-4

Schneider, N. M., & Trauger, J. T. (1995). The structure of the Io torus. *The Astrophysical Journal*, *450*, 450. https://doi.org/10.1086/176155

Shprits, Y., Menietti, J., Gu, X., Kim, K.-C., & Horne, R. (2012). Gyroresonant interactions between the radiation belt electrons and whistler mode chorus waves in the radiation environments of earth, jupiter, and saturn: A comparative study. *Journal of Geophysical Research*, *117*(A11). https://doi.org/10.1029/2012ja018031

Shprits, Y. Y., Menietti, J. D., Drozdov, A. Y., Horne, R. B., Woodfield, E. E., Groene, J. B., et al. (2018). Strong whistler mode waves observed in the vicinity of Jupiter's moons. *Nature Communications*, *9*(1), 3131. https://doi.org/10.1038/s41467-018-05431-x

Stix, T. H. (1992). *Waves in plasmas*. Springer Science and Business Media.

Teng, S., Tao, X., & Li, W. (2019). Typical characteristics of whistler mode waves categorized by their spectral properties using Van Allen Probes observations. *Geophysical Research Letters*, *46*(7), 3607–3614. https://doi.org/10.1029/2019gl082161

Tomás, A. T., Woch, J., Krupp, N., Lagg, A., Glassmeier, K.-H., & Kurth, W. S. (2004). Energetic electrons in the inner part of the Jovian magnetosphere and their relation to auroral emissions. *Journal of Geophysical Research*, *109*(A6). https://doi.org/10.1029/2004ja010405

Tsurutani, B. T., & Smith, E. J. (1974). Postmidnight chorus: A substorm phenomenon. *Journal of Geophysical Research*, *79*(1), 118–127. https://doi.org/10.1029/ja079i001p00118

Tsurutani, B. T., & Smith, E. J. (1977). Two types of magnetospheric ELF chorus and their substorm dependences. *Journal of Geophysical Research*, *82*(32), 5112–5128. https://doi.org/10.1029/ja082i032p05112

Vogt, M. F., Kivelson, M. G., Khurana, K. K., Walker, R. J., Ashour-Abdalla, M., & Bunce, E. J. (2014). Simulating the effect of centrifugal forces in Jupiter's magnetosphere. *Journal of Geophysical Research: Space Physics*, *119*(3), 1925–1950. https://doi.org/10.1002/2013ja019381

Waldrop, L., Roelof, E., & Fritz, T. (2015). Three-dimensional convective flows of energetic ions in Jupiter's equatorial magnetosphere. *Journal of Geophysical Research: Space Physics*, *120*(12), 10–506. https://doi.org/10.1002/2015ja021103

Wang, D., Shprits, Y. Y., Zhelavskaya, I. S., Agapitov, O. V., Drozdov, A. Y., & Aseev, N. A. (2019). Analytical chorus wave model derived from van allen probe observations. *Journal of Geophysical Research: Space Physics*, *124*(2), 1063–1084. https://doi.org/10.1029/2018ja026183

Wang, J.-Z., Bagenal, F., Wilson, R. J., Nerney, E., Ebert, R. W., Valek, P. W., & Allegrini, F. (2024a). Radial and vertical structures of plasma disk in Jupiter's middle magnetosphere. *Journal of Geophysical Research: Space Physics*, *129*(7), e2024JA032715. https://doi.org/10.1029/2024ja032715

Wang, J.-z., Ma, J.-n., Huo, Z.-x., Xiong, Y., & Tian, D. (2021). Statistical study of energetic electrons in Jupiter's inner magnetosphere by Juno/JEDI. *Advances in Space Research*, *67*(5), 1709–1720. https://doi.org/10.1016/j.asr.2020.11.032

Wang, X., Li, L., Jiang, X., Fry, P. M., West, R. A., Nixon, C. A., et al. (2024b). Cassini spacecraft reveals global energy imbalance of Saturn. *Nature Communications*, *15*(1), 5045. https://doi.org/10.1038/s41467-024-48969-9

Woodfield, E. E., Horne, R. B., Glauert, S. A., Menietti, J. D., & Shprits, Y. (2014). The origin of Jupiter's outer radiation belt. *Journal of Geophysical Research: Space Physics*, *119*(5), 3490–3502. https://doi.org/10.1002/2014ja019891

Yuan, C., Roussos, E., Wei, Y., Krupp, N., Liu, Z., & Wang, J. (2024). Galileo observation of electron spectra dawn-dusk asymmetry in the middle Jovian magnetosphere: Evidence for convection electric field. *Geophysical Research Letters*, *51*(1), e2023GL105503. https://doi.org/10.1029/2023gl105503

Yuan, C., Zuo, Y., Roussos, E., Wei, Y., Hao, Y., Sun, Y., & Krupp, N. (2021). Large-scale episodic enhancements of relativistic electron intensities in Jupiter's radiation belt. *Earth and Planetary Physics*, *5*(4), 314–326. https://doi.org/10.26464/epp2021037

Zhao, H., Ni, B., Li, X., Baker, D., Johnston, W., Zhang, W., et al. (2019). Plasmaspheric hiss waves generate a reversed energy spectrum of radiation belt electrons. *Nature Physics*, *15*(4), 367–372. https://doi.org/10.1038/s41567-018-0391-6